Journal of Molecular Catalysis A: Chemical 329 (2010) 36–43

Contents lists available at ScienceDirect

Journal of Molecular Catalysis A: Chemical

journal homepage: www.elsevier.com/locate/molcata

Probing Lewis acidity and reactivity of Sn- and Ti-beta zeolite using industrially important moieties: A periodic density functional study

Bhakti S. Kulkarni[a], Sailaja Krishnamurty[b], Sourav Pal[a,*]

[a] Physical Chemistry Division, National Chemical Laboratory, NCL, Pashan Road, Pune 411008, India
[b] Functional Materials Division, Electrochemical Research Institute (CECRI), Karaikudi 630 006, India

ARTICLE INFO

Article history:
Received 2 April 2010
Received in revised form 9 June 2010
Accepted 11 June 2010
Available online 18 June 2010

Keywords:
Lewis acidity
Beta zeolite
Periodic-DFT
Reactivity descriptors
Ligand-zeolite complex

ABSTRACT

The Lewis acidic nature and reactivity of two industrially important catalysts, viz., Sn and Ti substituted beta zeolite (T-BEA) are analyzed using a unique combination of structural parameters, energetics and reactivity descriptors. To achieve this purpose, we adsorb the industrially important moieties (L) namely NH_3, H_2O, CH_3OH, CH_3CN on the active sites of T-BEA. The calculations were performed using a periodic density functional method where the valence electrons are described using a plane wave basis set in conjunction with pseudo-potentials for the core electrons. The analysis of the structural properties of these complexes reveals that TO_4 shows typical characteristic splitting 120°/90°, close to bipyramidal geometry as compared to tetrahedral symmetry observed in the bare T-BEA. This is associated with small variations in the framework bond lengths (≥0.08 Å) and a substantially large variation of bond angles (≤10°) in all the ligand-zeolite complexes. Further in both cases of Sn and Ti substituted beta zeolite, ligand interacts at optimum inter-atomic bond distance. Our interaction energies show that adsorption of all ligand moieties is stronger at Sn center than that of Ti. In general, the order of stability of the different T-BEA adducts is $NH_3 > H_2O > CH_3OH > CH_3CN$. The ligand interaction is associated with the corresponding bond elongation and bond reduction of the adsorbed molecules on catalyst active site, which can be taken as measure of red or blue shifted frequencies. Finally, the global descriptors of reactivity justify the fact that soft acid, Sn-BEA, interacts strongly with soft bases following the Pearson's HSAB principle. However, hard acid, Ti-BEA interacts with soft bases to form a stable Lewis adduct. Furthermore, the HOMO–LUMO gap of all Sn-BEA–L adducts is lower than that of Ti-BEA–L adducts indicating to its higher Lewis acidic nature compared to Ti-BEA.

1. Introduction

In the development process of new, selective and recyclable eco-friendly catalyst, zeolite beta (BEA) was synthesized in 1967 [1]. Later, on successive resolution of beta structure, such as high Si/Al ratio and its large pore size (12-membered ring channel) [2,3] over CHA and TS-1, attracted a great industrial interest in organic chemical conversions [4–7]. It was successfully used for acid catalyzed reactions [4], catalytic cracking [6], aromatic and aliphatic alkylation [7]. Some of the industrially important reactions catalyzed by BEA are alcohol and alkane oxidation, olefin epoxidation, aromatics hydroxylation, and cyclohexanone ammoximation. The broad catalytic activity of this solid material was attributed to the presence of isolated tetrahedral T(IV) (T-site) atoms in the framework position.

Titanium is one of the important metals which have been incorporated into the zeolite framework of larger pore and into mesoporous molecular sieves [8]. An important development to this class of catalyst was the synthesis of aluminium-free-titanium beta zeolite in fluoride medium [9]. Thus, Ti incorporated BEA zeolite not only resulted in good adsorption and catalytic properties, but also it opened the possibility for introducing other Lewis acid metals into the beta zeolite framework. Consequently, Corma et al. introduced Sn in the BEA framework and it was shown to have better catalytic activity than Ti-BEA [10]. In addition to this Mal and Ramaswamy, for the first time, synthesized and characterized the Al-free–Sn-BEA [11]. The Sn-BEA showed singular activity for Bayer–Villiger (BV) oxidation reaction, Meerwein–Ponndorf–Verley reduction of aldehydes and Oppenauer's oxidation of alcohols (MPVO) [10a,12–14]. In addition, it was active for all reactions named above, all of them involving carbonyl compound. On the contrary, Ti-BEA showed no activity for BV oxidations. Sn was predicted, to be a stronger Lewis acidic site than the Ti, due to higher electro negativity of Sn than Ti. The isolated Sn(IV) in BEA was

* Corresponding author.
E-mail address: s.pal@ncl.res.in (S. Pal).

1381-1169/$ – see front matter © 2010 Elsevier B.V. All rights reserved.
doi:10.1016/j.molcata.2010.06.014

characterized by Sn MAS NMR and *in situ* EXAFS spectroscopy [12].

Since the catalytic properties are inherently connected to the structural properties of a site, there have been several studies attempting to understand the structural issues in these two zeolites. The various experiments successfully proved the tetrahedral coordination of tin atoms in the BEA framework [12]. However, the structural features of the local active sites in isomorphically substituted zeolites have not been well understood from the experimental techniques. This necessitates a theoretical investigation [15–17] so as to have a better understanding on the nature and the structure of the active sites and their respective reactivities. The periodic approach is the most correct model [18–20] and the only one able to account for long range effects and for constraints acting on a [TO_4] (where T stands for tetrahedral, T-site) unit and thus predicts the structural features more accurately. This was verified from one of our recent studies [21], where we had reported the structural and reactivity differences of the Ti-BEA and Sn-BEA using periodic-DFT.

The structural studies in the above paper revealed that the Sn and Ti atoms preferably occupy the T2 and/or the T1 sites among the nine in-equivalent T-sites of zeolite beta. The cohesive energy results demonstrate that the incorporation of Ti is more favorable than Sn in BEA. With the use of LUMO energies and the local Fukui Functions, we compared the Lewis acidity of these two substitutions and confirm the higher acidic nature of Sn. However, surprisingly, the Sn-BEA exhibited higher hydrophilicity than the Ti-BEA. Apart from the hydrophilic and/or hydrophobic nature comparison, we can take the water adsorption as the measure of the strength of Lewis acid base interaction. The strong interaction of the basic water molecule at the active Sn site than that of Ti assures its higher acidic nature.

The catalytic activity of a Lewis acid for oxidation is related to its ability to form acid–base adducts with either the substrate or the oxidizing agent, enhancing its reactivity. The formation of adduct implies an electron density transfer from the Lewis base to the Lewis acid which is directly proportional to the energy difference and degree of overlap between the occupied orbital of the base and the empty orbital of the acid. Therefore, the strength of a Lewis acid can be related to the energy of its LUMO in such a way that the lower the LUMO energy, the easier its interaction with a base molecule [21–24]. However, other factors influence the acid–base interaction. For example, one such factor is the HSAB (hard–soft acid–base) principle, which states that hard acids coordinate preferentially to hard bases and soft acids with soft bases [25,26]. Another factor to be considered is the possibility of back-donation of electron density from the Lewis acid to the unoccupied orbital of the Lewis base [21]. An interaction may or may not occur, depending on the energy difference and degree of overlap between the orbital involved [22]. Modification of the electronic levels of both the metal and the molecule, after the adsorption of a basic molecule on the metal center, should also be taken into account. Hence, the activity of a catalyst for a given reaction depends not only on the properties of the isolated active site, but also on the changes caused by its interaction with the reactant molecules [25,26]. This latter approach has been adopted by several experimentalists using *in situ* IR and EXAFS spectroscopies [12,18] and theoreticians [20,22,24,27–31] using simple adsorption model of basic moieties at catalyst active centers. The above mentioned parameters are analyzed in the present paper on metal substituted beta zeolite-ligand complexes.

In the past [20,24,27–31] main attention has been devoted to study of the Ti(IV) center reactivity in various zeolites such as TS-1, CHA ,etc., through the adsorption of NH_3 and H_2O. Bordiga et al. [27,32,33] study the adsorption of CD_3CN and pyridine on Ti centers of the TS-1. They confirm their results with the experimental vibrational spectra. Similarly, Corma and co-workers [28] performed the *in situ* IR and DFT calculations with deuterated acetonitrile to outline the peculiarities of Sn-BEA. However, most of these studies consider a cluster model approach. The main drawback of the cluster model in the characterization of T(IV) Lewis centers using adsorption model is twofold: (1) the high dilution of the T(IV), where T/Si is lower than 1/30 (here in BEA also we have only one T/Si ratio) and (2) the presence of the framework defects (Si vacancies) generating internal hydroxyl groups.

Hence, in our present paper, we execute periodic-DFT (p-DFT) for the interaction study of important basic moieties adsorbed at the active sites of Sn-BEA and Ti-BEA. To study the interaction, we consider the basic moieties such as NH_3, H_2O, CH_3OH, CH_3CN. The clear interest towards NH_3 and H_2O molecules is the direct comparison with previous results. In addition, the NH_3 molecule is used in ammoximation of cyclohexanone to give cyclohexanone oxime as reagent. Also it is a stronger base than the H_2O molecule which helps direct comparison due to the effect induced by the Lewis base of the increasing strength. The choice of other molecules such as CH_3OH and CH_3CN is justified by the important role played by these moieties in the industrial application of BEA. The Lewis acid–base adducts thus formed is taken as measure of strength of interactions to compare the acidity of Sn and Ti centers in the BEA. The results are in qualitative agreement with previous studies. The bond elongation, bond reduction of adsorbed bases and deformation of TO_4 moiety is reported in detail for each adduct. In particular, we also report the discrepancy played by the weak bonds such as hydrogen bond in predicting misleading strength of interaction for that of Sn-BEA. In addition, difference in the interaction energies for Sn-BEA and CH_3CN using periodic and cluster model is clearly highlighted.

The work is organized as follows: Section 2 elaborates the periodic model of T-BEA and the respective adducts formed after adsorption of L. Section 3 discourse the computation used to model and calculate the systems. Section 4 imparts the finding of these calculations, mainly, the comparative study of adsorption of the above mentioned basic moieties to study the deformation and hence resulted reactivity. Section 5 finally concludes the results.

2. Simulation model

In this simulation, we use the periodic-DFT (p-DFT) to built the Ti-BEA, Sn-BEA and their adducts with different basic molecules (L = NH_3, H_2O, CH_3OH, CH_3CN). The unit cell of BEA is shown in Fig. 1. BEA is highly siliceous material, with a three-dimensional pore system of 12-membered ring aperture. The unit cell of an ideal fully siliceous BEA consists of 192 atoms with 64 Si and 128 O atoms distributed within the tetragonal lattice of dimensions (12.6 Å × 12.6 Å × 26.2 Å. There are nine distinct crystallographically defined T-sites. We adopt the structure of the BEA from our earlier theoretical study [21b]. In our earlier analysis [21b], we found that the Sn and Ti atom occupy T2 and/or T1 crystallographic positions in BEA. Hence, in the rest of the calculations we use single substituted Sn at T2 and Ti at T1 positions. The interaction of basic molecules at the active site is very important, since it gives rise to geometric perturbation and the energetic differences. We tried the various possible approaches of the basic molecule at the active site. Many of these resulted in high energy and high force values. The most favorable ligand approach at the active T-site is along the b axis (see Fig. 2). This insertion gives rise to geometric distortion [27–29]. Schematic representation of T-BEA–L is given in Figs. 2 and 3. We built the same periodic environment i.e. size of unit cell, grid size etc for the T-BEA–L adducts and bare L molecules as that of the bare solid i.e. T-BEA.

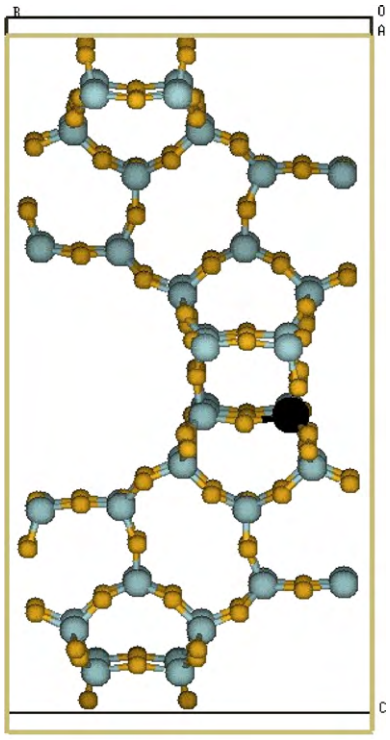

Fig. 1. The crystallographically defined BEA unit cell with Ti at T1 site. Black sphere: Ti atom, gray spheres: Si atoms, yellow spheres: O atoms. (For interpretation of the references to color in this figure legend, the reader is referred to the web version of the article.)

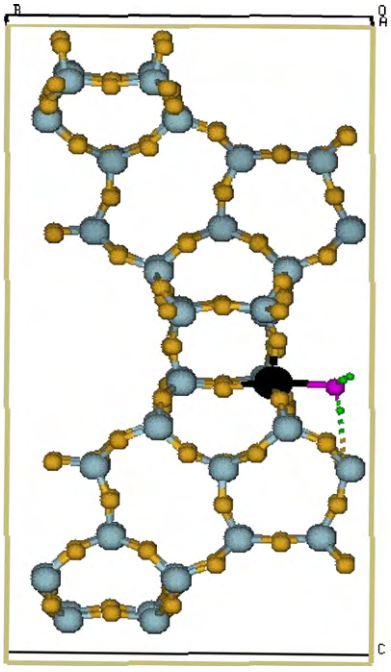

Fig. 2. Optimized T-BEA/NH_3. Black sphere: T atom, gray spheres: Si atoms, yellow spheres: O atoms, pink sphere: N atom and small green spheres: H atoms. (For interpretation of the references to color in this figure legend, the reader is referred to the web version of the article.)

3. Computational details

All the calculations are performed using VASP code which utilizes p-DFT [34]. The periodic boundary conditions facilitate one to add long range electrostatic interactions that are included in Ewald summations. Similar to normal DFT programs, the stationary ground state in p-DFT is calculated by solving Kohn-Sham equations. However, the most common practice of p-DFT programs to represent valence electrons is the use of plane waves (PW) in conjunction with pseudo-potentials (PP) for the core electrons. We use Vanderbilt's ultrasoft pseudo-potentials [35]. The optimized T-BEA model [21b] was employed as the starting geometry to study the interaction of T-BEA zeolite with all probes. The adducts so formed have been fully optimized at 500 eV PW basis cut-off without any geometrical constraints. The interactions thus obtained are further evaluated at 1000 eV cut-off considering single point convergence. The impact of high PW cut-off in the calculation of energy dependent properties, such as interaction energy, is recently illustrated in the literature [36]. The exchange-correlation functional is expressed by the generalized gradient approximation (GGA) with the Perdew-Wang 91 functional [37]. The calculations were restricted to the gamma point in the Brillouin zone sampling. The structural optimization of the Sn- and Ti-BEA has been carried out using conjugate gradient method. The optimization was considered to be achieved when the maximum force on the atoms was less than 0.08 eV/Å. One should note that during the optimization, the cell shape of the unit cell has been fully relaxed, while keeping its volume constant. This is due to the fact that the percentage of Sn and Ti in BEA is only 1/u.c. Similar optimization procedure is repeated for the calculation of Sn-BEA and Ti-BEA with all basic molecules, L, interacting at the Sn and Ti centers, respectively. The optimization of bare L moieties is derived with same computational procedure.

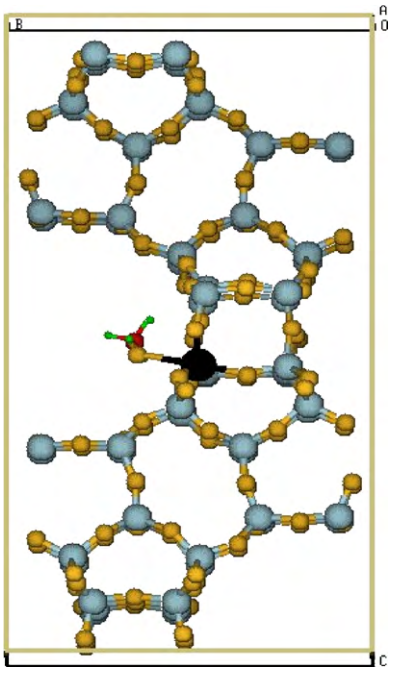

Fig. 3. Optimized T-BEA/CH_3OH. Black sphere: T atom, gray spheres: Si atoms, yellow spheres: O atoms, red spheres: C atoms and small green spheres: H atoms. (For interpretation of the references to color in this figure legend, the reader is referred to the web version of the article.)

4. Results and discussion: interaction of T-BEA with NH_3, CH_3CN, CH_3OH and H_2O

The least energetic approach of the ligand moieties on the active T-site in the BEA are shown in Figs. 2 and 3. The NH_3 and CH_3CN interact with Sn and Ti centers via N atom as shown in Fig. 2, where as CH_3OH and H_2O interact via O atom as shown in Fig. 3. This sec-

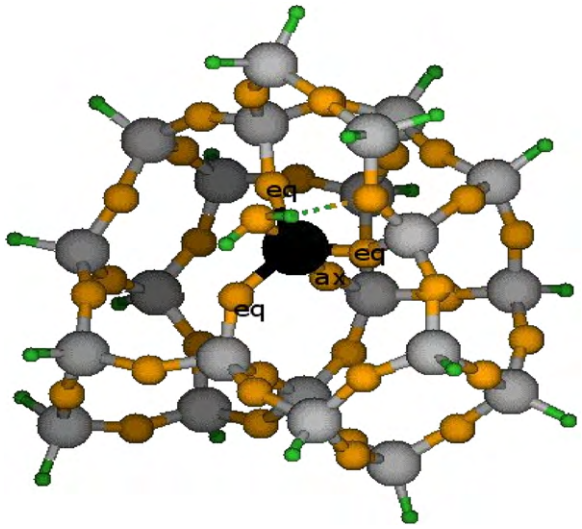

Fig. 4. Optimized T-BEA/H_2O showing axial (ax) and equatorial (eq) splitting of TO_4 unit. Black sphere: T atom, gray spheres: Si atoms, yellow spheres: O atoms, and small green spheres: H atoms. *Note*: An H atom of H_2O clearly shows hydrogen bonding with framework oxygen. (For interpretation of the references to color in this figure legend, the reader is referred to the web version of the article.)

tion first discusses the common structural features of all adducts and further it investigates the comparative interaction energy differences and predicts the trend of reactivity of all moieties with the respective catalyst. Following this with the help of global descriptors of reactivity, LUMO (of catalyst) and HOMO (of ligands) we will summarize the inter-reactivity trend for Sn and Ti substitutions.

4.1. Structural deformation of T-BEA framework upon ligand adsorption

Table 1 presents the optimized structural details and the reactivity descriptors of Sn-BEA and Ti-BEA. It should be noted that only the average bond distances and bond angles are presented. It can be seen from Table 1 that if we compare the Sn and Ti substitution in zeolite beta framework, we get expected order of ⟨T–O⟩ bond lengths, viz., Sn–O > Ti–O. On the other hand, the ⟨T–O–Si⟩ bond angles vary as Sn–O–Si < Ti–O–Si. The particular T–O bond length difference is due to the larger atomic size of Sn with respect to Ti. On the other hand, smaller sized Ti shows better angular flexibility with greater Ti–O–Si angle and consequently resulting in larger Ti–Si bond distance (by ∼0.04 Å from Sn–Si distance). Thus, the adaptation of the BEA framework to Sn and Ti substitution results in a quite localized deformation of a pure siliceous framework. Hence, we can infer that the difference in adsorption properties between Sn- and Ti-BEA should be mainly due to the electronic differences of these sites and the changes caused by the interacting reactant molecules. Detailed understanding on the structural differences between Sn- and Ti-BEA zeolite is available in one of our earlier studies [21b].

Table 2 presents the optimized structural parameters of T-BEA–L adducts. We can see that after the adsorption of ligand molecules at the reactive center, the corresponding framework T–O bonds undergo the following perturbation with respect to that of bare T-BEA: in the bare T-BEA, T atoms were in perfect tetrahedral environment, however, in their respective adducts the four framework oxygen atoms of TO_4 unit split into one axial, T–O_{ax}, opposite to the adsorbed ligand and three equatorial, T–O_{eq}. Consequently, the T–Si distances are also perturbed. Fig. 4 presents this detail splitting of the TO_4 unit. Table 2 gives this range of T–O and T–Si bond distances in the adducts. Here, the larger T–O bond length (or T–Si) corresponds to the respective T–O_{ax} bond (or T–Si_{ax}), thus, the oxygen atom which is exactly opposite to adsorbed ligand constitutes the most affected T–O (or T–Si) bond. However, the rest three T–O_{eq} (or T–Si_{eq}) bonds correspond to the smaller value of this range. The impact of tetrahedral symmetry loss by framework oxygen atoms is not just restricted to bond distances but it also disturbs the corresponding T–O–Si framework bond angles. The resulting range of T–O–Si bond angle is given in last column of Table 2. In both T-BEA–L adducts, the largest bond angle of this range belongs to T–O_{ax}–Si where as the smallest to T–O_{eq}–Si. The most disturbed framework bond angle is O–T–O. The total six O–T–O angles of the original T-BEA TO_4 unit gives rise to two triplets O_{eq}–T–O_{eq}, α, and O_{eq}–T–O_{ax}, β, angles. Table 2 highlights the fact that these triplets are also not equal but fall in a range. In addition to these bonds and angles formed by framework atoms, Table 2 also reports the hydrogen bond (H_L–O_T) formed between framework oxygen (O_T) and ligand hydrogen (H_L). Here, the bracketed values indicate the number of hydrogen bonds formed by ligand hydrogens. These structural deformations in the complexes are commonly seen in case of all ligands.

Coming to the details of the structural deformations, the T–O bonds in the respective T-BEA–L adduct show elongation to an equal extent. Thus, irrespective of the nature of adsorbed ligand, Ti–O_{ax} and Ti–O_{eq} comprise to 1.88 and 1.80 Å, respectively. Similarly, the Sn–O_{ax} and Sn–O_{eq} bonds correspond to 1.99 and 1.89 Å. The adsorption of L causes on an average 0.081 and 0.083 Å elongation of T–O_{ax} distance in Ti-BEA and Sn-BEA adduct, respectively. However, the rest three T–O_{eq} bonds are closer to the T–O bonds of the bare T-BEA. Thus, we note an equal perturbation of T–O bonds in both the Sn- and Ti-BEA framework upon interaction with all ligands. The average variations of Ti–O bonds reported above agree well with the EXAFS data [32,33]. Interestingly, earlier cluster calculations [38] also report a similar range of variations. Accordingly, the T–Si bond distances also show variation in the T-BEA–L complexes compared to the bare T-BEA. Unlike T–O_{eq} bonds, T–Si_{eq} bonds optimize to lower bond lengths compared to T–Si distances present in the bare T-BEA. Once again, irrespective of ligand nature and metal active center, T–Si_{eq} bond reduces by ∼0.04 Å. However, the T–Si_{ax} bond further elongates by ∼0.14 and ∼0.18 Å in respective Ti- and Sn-BEA adducts. The Sn-BEA–CH_3OH adduct is exception here, where the Sn–Si_{eq} bond show strong reduction where as the Sn–Si_{ax} bond result in shorter elongation.

As discussed, hydrogen bond (H_L–O_T) is observed between the ligand hydrogen (H_L) and framework oxygen (O_T). At T1 site (Ti substituted site) these hydrogen bonds formed are shorter in bond length but at T2 site (Sn substituted site) these bonds result in weak bonding. In the case of Ti-BEA–NH_3 adduct, we report strong hydrogen bond of 2.23 Å which later on results in elevated interaction energy of NH_3 with Ti center as will be elaborated in next section. The most important inter-molecular bond length, distance between active site of zeolite and interacting atom of adsorbed ligand, T–L, is reported in Table 2. It is seen from the table that NH_3 molecule is optimized at a distance of 2.35 Å from the Ti center (T1 site) of BEA, being slightly shorter (about 0.017 Å) compared to that obtained on the Ti-CHA model [26b]. The Sn-BEA–NH_3 distance optimizes at 2.38 Å. Similarly, the CH_3CN interaction optimizes at 2.35 and 2.38 Å from Ti and Sn centers of BEA, respectively. In general, the ligands containing oxygen atom as donor atom converge to longer inter-molecular bond. The CH_3OH optimizes, respectively, to 2.46 and 2.44 Å at Ti and Sn centers. The Sn-BEA–OH_2 inter-molecular bond optimizes at 2.38 Å. The Ti-BEA–OH_2 bond length optimizes at 2.44 Å.

To conclude, the Ti–O–Si bond angles, which range between 144° and 163°, are larger than the Sn–O–Si angles (142–159°). This can be attributed to the angular flexibility of small sized Ti. This angle reduces exceptionally during the formation of Sn-BEA–CH_3OH adduct. In addition, ligand approach at active T2 site

Table 1
Optimized structural parameters of Sn-BEA and Ti-BEA.

T	T–O (Å)	T–Si (Å)	T–O–Si (°)	HOMO (eV)	LUMO (eV)	Δ(H–L) (eV)
Ti	1.80	3.3	151.7	−3.13	1.42	−4.55
Sn	1.91	3.34	144.2	−3.12	1.37	-4.49

Average T–O bond lengths, T–Si bond distances, T–O–Si bond angles and the HOMO, LUMO energies.

is more linear, L–T–O_T angle being close to 180°, where as same angle at T1 site is close to ∼170° (see Fig. 4). Consequently, six O–T–O angles in the respective adduct of Sn- and Ti-BEA split to different extent. The order of O–T–O angle splitting vary with respect to strength of ligand as NH_3 > CH_3CN > CH_3OH. Thus, the structural study of adducts conjecture that irrespective of the ligand nature, the bond length variation of the framework atoms is restricted in fixed range, however, bond angles deviates to different magnitudes. Similarly, irrespective of the catalyst active center, Sn or Ti, ligand interacts at optimum bond distance.

4.2. Energetics of interacting T-BEA and ligands (L)

In this subsection, we discuss the strength of interaction of various ligands with Sn-BEA and Ti-BEA so as to highlight the distinct Lewis acidic nature of Sn and/or Ti centers. For this purpose, we calculate the interaction energy defined as the difference between the energy of adduct formed at equilibrium and the energy of the constituent molecules in their ground state. This is calculated as follows,

$$\text{Interaction energy}(E_{\text{int}}) = (E_{\text{T-BEA}} + E_{\text{L}}) - E_{\text{T-BEA–L}} \quad \text{(I)}$$

In our earlier investigation on the hydrophilicity of Sn- and Ti-BEA [21b], we showed that the energy of H_2O interaction with Sn-BEA is 0.3323 eV and that of with Ti-BEA is 0.1342 eV. The Sn site in BEA is more hydrophilic compared to Ti site. This also confirms the higher Lewis acidic nature of Sn-BEA. As the water is the most common reaction medium, H_2O gains extreme importance in determining the catalyst activity study. Thus, water not only coordinates with catalyst active center but many times poisons the site and reduces its reactivity. Here, we do not consider the structural details of the T-BEA and H_2O adduct. The geometric features concerning the T-BEA–H_2O adducts are reported by us in the earlier study [21b]. For detailed interest one can refer to this study. We are going to extrapolate the analysis of this exothermic interaction of water to analyze the interaction of all ligands with both the Sn and Ti centers. The interaction energy of all ligands with Sn- and Ti-BEA is reported in Table 3. The interaction energies reported in bracket are calculated at high PW cut-off of 1000 eV.

By the simple chemist intuition, we expect the higher acidic Sn center to result in stable interaction with the strong base NH_3 to form a better Lewis adduct than the less acidic Ti center. However, interaction energies of NH_3 ligand with the Sn and Ti substituted beta zeolite contradict these findings. Table 3 highlights the increase of interaction energy by 0.02 eV (0.06 eV at 1000 eV PW cut-off), while going from Sn to Ti center. Although this increase in the interaction energy is not considerable, we attribute this discrepancy to the distortion in the local environment after the adsorption of NH_3 as discussed below. The interaction of NH_3 is considered at T1 site of Ti-BEA where as for Sn-BEA it is at T2. Although the Sn–O–Si bond angles are smaller than Ti–O–Si, the Ti center shows better angular flexibility due to its small atomic radius [21b]. As a result, hydrogen bond formed between the framework oxygen and the ligand hydrogen atoms (NH_3) is retained during the optimization. However, due to lack of Sn–O–Si angular flexibility there is no such hydrogen bonding observed for the adsorbed NH_3 in the case of Sn-BEA (ref. Table 2). The H_L–O_T bond lengths are reported in Table 2. The shortest bond distance between hydrogen atom of ammonia and framework oxygen in Ti-BEA–NH_3 adduct is 2.24 Å where as same for Sn-BEA–NH_3 adduct is 2.72 Å. This strong hydrogen bonding interaction of Ti-BEA–NH_3 adduct reflects in step up interaction energy compared to Sn-BEA–NH_3 adduct. We also carry a test calculations of NH_3 interacting with Sn-BEA, where, Sn is now substituted at T1 site. Surprisingly, interaction energy is 0.78 eV (an increase of 0.49 eV from its T2 site). At T1 site, Sn-BEA–NH_3 does not fail to count the strong hydrogen bond. The shortest hydrogen bond thus formed is 2.33 Å and NH_3 optimizes at shorter bond length of 2.33 Å. Therefore, though the structural arrangement of atoms look equivalent in the unit cell model of BEA, the electronic difference in local environment of the active site plays an extensively important role in deciding materials catalytic behavior. The corresponding adsorbed N–H bonds are very weakly elongated in Ti-BEA–NH_3 adduct (about 0.001 Å). On the other hand, elongation is about 0.016 Å for Sn-BEA–NH_3 adduct. This elongation of interacting ligand N–H bond can be taken as evidence of red shift in IR frequency and hence measure of strength of interaction at catalyst active site.

An earlier experimental study of the vibrational properties of CH_3CN adsorbed on different zeolite, TS-1, as an evidence for the presence of Lewis acidic centers [27] associated with Ti(IV) was given by Bonino et al. They found that acetonitrile forms a labile adduct with the Ti of TS-1 with a $\Delta\upsilon$(CN) stretching frequency of +37 cm^{-1}. Analogous experiment on Sn-BEA has been recently carried out by Corma and co-workers [28,29]. Their study also predicted a blue shifted $\Delta\upsilon$(CN) stretching frequency of +42 cm^{-1}. In addition, to study the structure-activity relation of catalyst they had carried out a computational study based on a cluster model approach. Interestingly, their model comprised of various reaction sites and various neighboring groups. For the comparison purpose, we restrict ourself to pure siliceous environment of Sn center and do not consider their hydrolyzed model. In line with their frequency analysis, the CN distance in our calculation passes from 1.161 Å (bare one) to 1.156 Å (engaged one) predicting blue shift of the υ(CN) stretching frequency. This result is in qualitative agreement with the results reported in previous literature [27–29]. In particular, the interaction of probe molecule such as acetonitrile with Lewis acid center involves electron density transfer from lone pair

Table 2
Optimized structural parameters of T-BEA–L adducts.

Adducts	T–O (Å)	T–Si (Å)	T–L (Å)	H_L–O_T (Å)	α (°)	β (°)	T–O–Si (°)
NH_3/Ti	1.80–1.88	3.24–3.45	2.35	2.23 (1)	110.9–131.2	95.0–104.9	144.1–161.9
NH_3/Sn	1.89–1.99	3.29–3.53	2.38	2.71 (0)	105.8–137.3	95.5–103.4	142.3–159.4
CH_3CN/Ti	1.79–1.88	3.29–3.45	2.35	2.45 (0)	110.1–125.5	93.9–102.5	146.6–163.2
CH_3CN/Sn	1.89–1.99	3.31–3.52	2.38	2.90 (0)	107.0–129.1	94.0–107.0	142.3–158.4
CH_3OH/Ti	1.80–1.86	3.26–3.43	2.46	2.54 (1)	111.3–123.7	102.4–105.9	146.4–160.2
CH_3OH/Sn	1.89–1.98	3.22–3.45	2.44	2.57 (1)	106.6–129.8	100.6–103.5	141.4–150.1

Table 3
HOMO, LUMO energies of Lewis bases and T-BEA–L adducts.

Systems	E_{int} (eV)	HOMO (eV)	LUMO (eV)	Δ(H–L) (eV)
NH_3	–	−6.03	−0.80	−5.23
NH_3/Ti	0.3156 (0.3459)	−2.69	1.43	−4.12
NH_3/Sn	0.2963 (0.2825)	−2.78	1.91	−4.70
CH_3CN	–	−8.10	−0.85	−7.25
CH_3CN/Ti	0.0325 (0.0083)	−2.80	1.36	−4.15
CH_3CN/Sn	0.1607 (0.1074)	−2.84	2.11	−4.95
CH_3OH	–	−6.33	−0.75	−5.58
CH_3OH/Ti	0.0716 (0.0980)	−2.65	1.43	−4.08
CH_3OH/Sn	0.2951 (0.3016)	−2.80	1.77	−4.57

of nitrogen to the catalyst LUMO, as a result CN bond reduces and υ(CN) frequency shifts to higher value. The computed blue shift, accompanied by a reduction of −0.005 Å of the C–N distance (compared to bare CN distance), proves the strong adsorption of the CH_3CN on the T-BEA active centers. This fact is well reproduced in the interaction energy calculation with the both T substituted BEA. Although, the cluster model predicted T–L bond lengths match well with our periodic model the interaction energy values differ from ours [28]. The interaction energy of Sn-BEA with CH_3CN predicted by the cluster model approach was 0.3 kcal/mol [28]. However, the additive long range interactions covered in periodic model results in an interaction energy increase of 3.45 kcal/mol. This difference can be attributed to the additive interaction. The interaction energy of CH_3CN with Ti-BEA adduct is 0.032 eV (0.008 eV at 1000 eV PW cut-off). Thus, the interaction of Sn-BEA is stronger with CH_3CN than that of Ti-BEA.

The CH_3OH is reagent of prime interest in several industrial reactions. The lone pair present on the O atom of CH_3OH should be more attractive towards the positive centers present in substituted BEA. Similar to CH_3CN interaction, the interaction energies computed for Sn-BEA, Ti-BEA and CH_3OH show large differences. The Sn-BEA and CH_3OH interaction is stronger and turns out to be 0.295 eV (0.301 eV at 1000 eV PW cut-off). On the other hand, the Ti-BEA and CH_3OH interaction energy is 0.0716 eV (0.098 eV at 1000 eV PW cut-off). In the optimized structure of Ti-BEA–CH_3OH, C–O bond is 1.46 Å and O–H bond is 0.97 Å (i.e. elongates to +0.02 and +0.006 Å with respect to bare molecule). For Sn-BEA adduct, the C–O bond shows elongation by 0.013 Å and OH bond by 0.003 Å. The computed elongations can be accounted as measure of adsorption of CH_3OH on the active centers, resulting in the red shifted frequencies. This is a consequence of structural differences around T1 and T2 sites of the beta zeolite.

The present energetics of ligand interaction reveals that all the basic moieties result in exothermic interaction with Sn and Ti sites. Furthermore, the higher interaction energies of Sn-BEA–L adducts confirm their stability compared to Ti-BEA–L adducts. The ligand interaction is associated with the respective bond elongation and bond reduction of the adsorbed molecules on catalyst active site, which can be taken as measure of red or blue shifted frequencies. In general, the order of stability of the different T-BEA adducts is $NH_3 > H_2O > CH_3OH > CH_3CN$. For Sn-BEA, this order is slightly reversed, viz., the H_2O interacts strongly with Sn-BEA compared to NH_3. However, in next section of reactivity descriptors, frontier orbital energies, justify the permanence of these respective interactions. The interactions of CH_3CN and CH_3OH are almost negligible with Ti-BEA. In conclusion, the higher acidic Sn site interacts strongly with all basic moieties compared to lesser acidic Ti site.

4.3. Reactivity of T-BEA towards ligands (L)

We have applied the HSAB principle to understand the reactivity of Sn- and Ti-BEA towards ligand moieties. Pearson formulated the concept of HSAB principle for understanding reactivity of chemical systems and their interactions [25,26]. This gave a new insight in interpreting the reactivity of chemical systems on the basis of their HOMO and LUMO energies [25,26]. Thus a system can be categorized as soft acid (SA) with low-lying LUMO, soft base (SB) with high lying HOMO and hard acid (HA) with high lying LUMO where as hard base (HB) with low-lying HOMO. It has been well established that the interactions between SA–SB are covalent, HA–HB are ionic and SA–HB or HA–SB are mostly weak electrostatic and form Lewis adducts. Here, we must recall that the Lewis acidity, being related with an electron acceptor character, can be related with the global affinity of the solid [21b,22,23]. Qualitatively, LUMO energies can be used for a comparison between electron affinities of Sn- and Ti-BEA. The HOMO and the LUMO energies and their respective HOMO–LUMO gaps of Sn- and Ti-BEA are revised [21b] in Table 1. Globally the LUMO energy of Sn substituted BEA zeolite is lower than that of the Ti ones. Also the corresponding HOMO–LUMO gap of Sn-BEA is small which correlates this solid to a larger global softness. Thus, the Sn-BEA results in the most Lewis acidic and softer solid, hence, more reactive catalyst.

Table 3 describes the HOMO, LUMO energies, and the corresponding HOMO–LUMO gaps of all the ligand molecules. We observe decreasing order of HOMO energies of all the ligands as: H_2O (−5.99 eV) > NH_3 > CH_3OH > CH_3CN. Thus, here CH_3CN lead to hard base and rest three bases are soft bases based on their closely lying HOMO energies. However, NH_3 and H_2O are of equal strength. This is in line with our interaction energy analysis of the different T-BEA adducts ($NH_3 > H_2O > CH_3OH > CH_3CN$) where we get less adsorption energy of CH_3CN with both Sn- and Ti-BEA. However, soft bases namely H_2O and NH_3 interact strongly with Sn and Ti-BEA. The global descriptors of reactivity thus explain the fact that soft acid, Sn-BEA, interacts strongly with soft bases H_2O, NH_3 and CH_3OH to give a covalent complex where as hard acid, Ti-BEA interacts with same bases to form a stable Lewis adduct. In addition, according to the above definition, interaction between CH_3CN with Ti-BEA is weakly ionic (see Table 3: interaction energy is negligible) where as interaction of CH_3CN with Sn-BEA is weakly electrostatic (Lewis acid–base adduct) in nature. In general, interaction of Sn-BEA is strong with all ligands compared to Ti-BEA (compare interaction energies of respective adducts). Table 3 also summarizes the HOMO–LUMO gaps of all T-BEA–L adducts. The HOMO–LUMO gap of all Sn-BEA–L adducts is lower than that of Ti-BEA–L adducts. This thus explains the greater stability of all Sn-BEA–L complexes. Hence, we can once again state that globally Sn-BEA zeolite results in higher Lewis acidic catalyst forming stable interaction with all basic molecules than the Ti-BEA zeolite. Other reactivity descriptors such as chemical potential, hardness and philicity of a molecule are also added in Table 4 for the sake of completeness. However, it may be noted that none of these descriptors follow the trend reported by the interactions energies. The reason for this may be attributed to the sensitivity of these descriptors which applies to periodic density functional methods.

In addition to highlight the charge transfer in the interactions of T-BEA and L, we include a short discussion with the help of difference charge density ($\Delta\rho$) plots. The $\Delta\rho$ plots for each type of interaction, viz., covalent, Lewis adduct and ionic are reported in

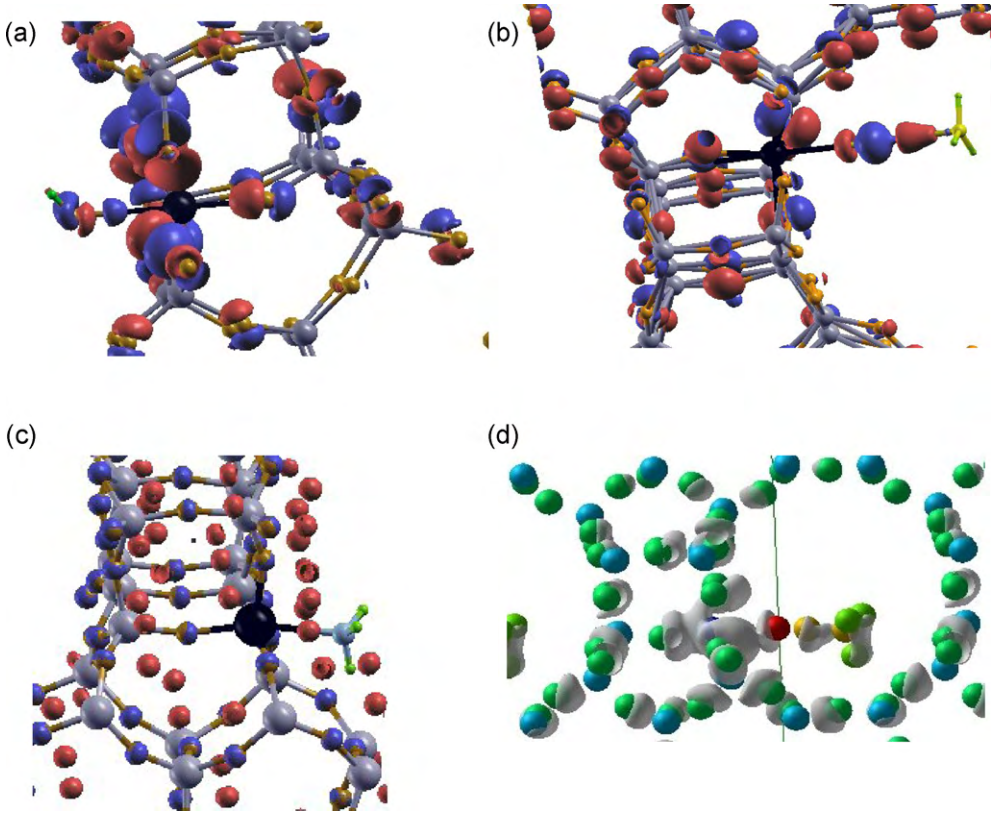

Fig. 5. (a) Sn-BEA–H_2O: SA–SB, covalent interaction indicated by presence of blue sphere along inter-molecular bond. (b) Sn-BEA–CH_3CN: SA–HB, weakly electrostatic interaction indicated by red sphere along inter-molecular bond. (c) Ti-BEA–NH_3: HA–SB, weakly electrostatic interaction indicated by red sphere along inter-molecular bond. (d) Ti-BEA–CH_3CN: HA–HB, ionic interaction indicated by polarization of density along inter-molecular bond. (For interpretation of the references to color in this figure legend, the reader is referred to the web version of the article.)

Fig. 5. Here, the blue signifies charge gain where as red represents charge depletion. Fig. 5a shows SA–SB, Sn-BEA–H_2O interaction. The charge transfer between H_2O and Sn is indicated by small blue sphere. The blue sphere along inter-molecular bond, here, represents the bond critical point which can be taken as measure of a strong bonding such as covalent interaction. Fig. 5b and c shows, SA–HB and HA–SB, Lewis acid–base interactions forming Lewis adducts. As discussed in the beginning of this section these interactions are weakly electrostatic in nature and this is well reflected in their $\Delta\rho$ plots. The presence of small red sphere along the inter-molecular bonding space here denotes loss of charge where as blue sphere on ligand donor atom indicates concentration of charge density on it. Similarly, HA–HB, Ti-BEA–CH_3CN, ionic interaction is shown in Fig. 5d (for clear visualization not color coded). Fig. 5d clearly shows a polarized charge density between Ti-BEA–CH_3CN bonding region which is an indication of ionic bond. Both the atoms, Ti – blue sphere and N – red sphere, show polarization of electronic densities on them.

Table 4
Chemical potential, hardness and philicity descriptors for L and T-BEA–L.

Systems	μ	η	ω
NH_3	−3.42	−2.62	−2.23
CH_3OH	−3.54	−2.79	−2.25
CH_3CN	−4.48	−3.63	−2.76
NH_3/Sn	−0.44	−2.35	−0.04
CH_3OH/Sn	−0.61	−2.04	−0.09
CH_3CN/Sn	−0.37	−2.48	−0.03
NH_3/Ti	−0.63	−2.06	−0.1
CH_3OH/Ti	−0.52	−2.29	−0.06
CH_3CN/Ti	−0.72	−2.08	−0.12

5. Conclusion

The reported geometries of the substituted beta and their respective interactions with NH_3, H_2O, CH_3OH and CH_3CN are obtained with the plane wave basis code VASP. Catalyst active site T2 and T1 are substituted by Sn and Ti, respectively. All the interactions are fully optimized without any geometrical constraints. The geometric and energetic deformations are discussed successfully using p-DFT.

In the bare T-BEA, TO_4 moiety is quite near to tetrahedral symmetry [21b,27,39]. However, the results discussed here predict the deformation of TO_4 moiety due to adsorption of basic molecules. In the optimized ligand adsorbed adducts, TO_4 shows typical characteristic splitting 120°/90° there by resulting into a nearly bipyramidal geometry. Irrespective of the adsorbed ligand nature, the bond length variation of the framework atoms is restricted in fixed range while the bond angles exhibit a larger variation. Similarly, irrespective of the catalyst active center, Sn or Ti, ligand interacts at an optimum bond distance. The interaction energy results demonstrate that all the basic moieties results in exothermic interaction with Sn and Ti sites. Furthermore, the higher interaction energies of Sn-BEA–L adducts confirm their stability compared to Ti-BEA–L adducts. This strength of interaction is also associated with a corresponding bond elongation and/or bond reduction of the adsorbed molecules on the catalyst active site, which can be taken as measure of red or blue shifted frequencies [27,32,33]. In general, the order of stability of the different T-BEA adducts is $NH_3 > H_2O > CH_3OH > CH_3CN$. For Sn-BEA, this order is slightly reversed. The H_2O interacts strongly with Sn-BEA compared to NH_3. Overall the interaction of ligands with Sn and Ti substituted beta zeolite depend on a delicate balance of several

factors such as substitution site of metal, angular flexibility around those sites and weak interactions like hydrogen bonds. All these factors reflect in global reactivity descriptors. The global descriptors of reactivity justify the fact that soft acid, Sn-BEA, interacts strongly with soft bases H_2O, NH_3 and CH_3OH to give a covalent complex where as hard acid, Ti-BEA interacts with same bases to form a stable Lewis adduct. In addition, the interaction energies and reactivity descriptors of Ti-BEA–CH_3CN complex indicates it to be weakly ionic where as interaction of CH_3CN with Sn-BEA is weakly electrostatic in nature. The $\Delta\rho$ plots support these findings. The HOMO–LUMO gap highlights the greater stability of all Sn-BEA–L complexes which once again address the higher Lewis acidic nature of Sn-BEA than Ti-BEA.

Acknowledgments

One of the authors (BSK) acknowledges CSIR (Council of Scientific and Industrial Research) for funding of the SRF (Senior Research Fellowship). We acknowledge the Center of Excellence in Scientific Computing at NCL. SP acknowledges the J.C. Bose Fellowship grant of DST towards partial fulfillment of this work.

References

[1] R.L Wadlinger, G.T. Kerr, E.J. Rosinski. U.S. Patent 3,308,069, 1967.
[2] J.M. Newsam, M.M.J. Treacy, W.T. Koestsier, C.B. de Gruyter, Proc. R. Soc. Lond. A420 (1988) 375.
[3] (a) A. Corma, M.T. Navarro, F. Rey, J. Rius, S. Valencia, Angew. Chem. Int. Ed. 40 (2001) 2277;
(b) A. Corma, M.T. Navarro, F. Rey, S. Valencia, Chem. Commun. (2001) 1486.
[4] G. Bellusi, G. Pazzuconi, C. Perego, G. Girotti, G. Terzoni, J. Catal. 157 (1995) 227.
[5] (a) J.A. Martens, J. Perez-Pariente, E. Sastre, A. Corma, P.A. Jacobs, Appl. Catal. 45 (1988) 85;
(b) P. Ratnasamy, R.N. Bhat, S.K. Pokhriyal, S.G. Hagde, R. Kumar, J. Catal. 119 (1989) 65.
[6] L. Boretto, M.A. Camblor, A. Corma, J. Perez-Pariente, J. Appl. Catal. 82 (1992) 37.
[7] A.J. Hoefnagel, H. van Bekkum, Appl. Catal. A 97 (1993) 87.
[8] A. Corma, J.L. Jorda, M.T. Navarro, F. Rey, Chem. Commun. (1998) 1899.
[9] T. Blasco, M.A. Camblor, A. Corma, P. Esteve, J.M. Guil, A. Martinez, J.A. Perdigon-Melon, S. Valencia, J. Phys. Chem. B 102 (1998) 75.
[10] (a) A. Corma, L.T. Nemeth, M. Renz, S. Valencia, Nature 412 (2001) 423;
(b) A. Corma, M.E. Domine, L.T. Nemeth, S. Valencia, J. Am. Chem. Soc. 124 (2002) 3194.
[11] N.K. Mal, A.V. Ramaswamy, Chem. Commun. 425 (1997).
[12] S.R. Bare, S.D. Kelly, W. Sinkler, J.J. Low, F.S. Modica, S. Valencia, A. Corma, L.T. Nemeth, J. Am. Chem. Soc. 127 (2005) 12924.
[13] (a) A. Corma, V. Fornes, S. Iborra, M. Mifsud, M. Rez, J. Catal. 221 (2004) 67;
(b) A. Corma, S. Iborra, M. Mifsud, M. Renz, J. Catal. 223 (2005) 96;
(c) A. Corma, M. Renz, Chem. Commun. (2004) 550.
[14] (a) A. Corma, M.E. Domine, L. Newmeth, S. Valencia, J. Am. Chem. Soc. 124 (2002) 3194;
(b) A. Corma, M.E. Domine, L. Nemeth, S. Valencia, J. Catal. 215 (2003) 294.
[15] I. Pbpai, A. Goursot, F. Fajula, J. Phys. Chem. 98 (1994) 4654.
[16] (a) N. Jardillier, D. Berthomieu, A. Goursot, J.U. Reveles, A.M. Koster, J. Phys. Chem. B 110 (2006) 18440;
(b) A. Martınez, A. Goursot, B. Coq, G. Delahay, J. Phys. Chem. B 108 (2004) 8823.
[17] (a) S. Krishnamurty, T. Heine, A. Goursot, J. Phys. Chem. B 107 (2003) 5728;
(b) T. Heine, A. Goursot, G. Seifert, J. Weber, J. Phys. Chem. A 105 (2001) 620.
[18] K. Sun, W. Su, F. Fan, Z. Feng, T.A.P.J. Jansen, R.A. van Santen, C. Li, J. Phys. Chem. A 112 (2008) 1352.
[19] (a) M. Kubo, Y. Oumi, H. Takaba, A. Chatterjee, A. Miyamoto, J. Phys. Chem. B 103 (1999) 1876;
(b) K. Teraishi, M. Ishida, J. Irisawa, M. Kume, Y. Takahashi, T. Nakano, H. Nakamura, A. Miyamoto, J. Phys. Chem. B 101 (1997) 8079.
[20] (a) E.A. Pidko, P. Mignon, P. Geerlings, R.A. Schoonheydt, R.A. van Santen, J. Phys. Chem. C 112 (2008) 5510;
(b) F. Tielens, J.F.M. Denayer, I. Daems, G.V. Baron, W.J. Mortier, P. Geerlings, J. Phys. Chem. B 107 (2003) 11065.
[21] (a) S. Shetty, S. Pal, D.G. Kanhere, A. Goursot, Chem. Eur. J. 12 (2006) 518;
(b) S. Shetty, B.S. Kulkarni, S. Pal, D.G. Kanhere, A. Goursot, J. Phys. Chem. B 112 (2008) 2573.
[22] (a) M. Boronat, A. Corma, M. Renz, G. Sastre, P.M. Viruela, Chem. Eur. J. 12 (2006) 7067;
(b) M. Boronat, A. Corma, M. Renz, G. Sastre, P.M. Viruela, Chem. Eur. J. 11 (2005) 6905.
[23] G. Sastre, A. Corma, Chem. Phys. Lett. 302 (1999) 447.
[24] A.M. Vos, K.H.L. Nulens, F. De Proft, R.A. Schoonheydt, P. Geerlings, J. Phys. Chem. B 106 (2002) 2026.
[25] R.G. Parr, R.G. Pearson, J. Am. Chem. Soc. 105 (1983) 7512.
[26] R.G. Pearson, J. Am. Chem. Soc. 85 (1963) 3533.
[27] (a) F. Bonino, A. Damin, S. Bordiga, C. Lamberti, A. Zecchina, Langmuir 19 (2003) 2155;
(b) A. Damin, S. Bordiga, C. Lamberti, A. Zecchina, K. Doll, J. Chem. Phys. 118 (2003) 10183.
[28] M. Boronat, P. Concepcion, A. Corma, M. Renz, Catal. Today 121 (2007) 39.
[29] M. Boronat, P. Concepcion, A. Corma, M.T. Navarro, M. Renz, S. Valencia, Phys. Chem. Chem. Phys. 11 (2009) 2876.
[30] I. Phpai, A. Goursot, F. Fajula, D. Plee, J. Weber, J. Phys. Chem. 99 (1995) 12925.
[31] (a) E.L. Meijer, R.A. van Santen, A.P.J. Jansen, J. Phys. Chem. A 103 (1999) 2553;
(b) E.H. Teunissen, A.P.J. Jansen, R.A. van Santen, J. Phys. Chem. 99 (1995) 1873;
(c) A.G. Pelmenschikov, R.A. van Santen, J. Phys. Chem. 97 (1993) 10678.
[32] (a) S. Bordiga, A. Damin, F. Bonino, A. Zecchina, G. Spano, F. Rivetti, V. Bolis, C. Prestipino, C. Lambeti, J. Phys. Chem. B 106 (2002) 9892;
(b) T. Blasco, M.A. Camblor, A. Corma, P. Esteve, J.M. Guil, A. Martinez, J.A. Perdigon-Melon, S.J. Valencia, J. Phys. Chem. B 102 (1998) 75;
(c) A. Zecchina, S. Bordiga, G. Spoto, A. Damin, G. Berlier, F. Bonino, C. Prestipino, C. Lamberti, Top. Catal. 21 (2002) 67.
[33] (a) V. Bolis, S. Bordiga, C. Lamberti, S. Zecchina, F. Rivetti, G. Spano, G. Petrini, Langmuir 15 (1999) 5753;
(b) V. Bolis, S. Bordiga, C. Lamberti, S. Zecchina, A. Carati, F. Rivetti, G. Spano, G. Petrini, Macropor. Mater. 30 (1999) 67.
[34] (a) G. Kresse, J. Hafner, Phys. Rev. B 48 (1993) 13115;
(b) G. Kresse, J. Furthermuller, Comput. Mater. Sci. 6 (1996) 15.
[35] D. Vanderbilt, Phys. Rev. B 41 (1990) 7892.
[36] B.S. Kulkarni, S. Krishanamurti, S. Pal, Chem. Phys. Lett. 484 (2010) 374.
[37] J.P. Perdew, Y. Wang, Phys. Rev. B 45 (1992) 13244.
[38] A. Damin, F. Bonino, G. Ricchiardi, S. Bordiga, A. Zecchina, C. Lamberti, J. Phys. Chem. B 106 (2002) 7524.
[39] M. Renz, T. Blasco, A. Corma, V. Formes, R. Jensen, L. Nemeth, Chem. Eur. J. 8 (2002) 4708.